



## Formation and thermodynamic stability of (polymer + porphyrin) supramolecular structures in aqueous solutions



Viviana C.P. da Costa, Barrington J. Hwang, Spencer E. Eggen, Megan J. Wallace, Onofrio Annunziata\*

Department of Chemistry, Texas Christian University, Fort Worth, TX 76129, USA

### ARTICLE INFO

#### Article history:

Received 20 December 2013  
Received in revised form 26 February 2014  
Accepted 27 February 2014  
Available online 11 March 2014

#### Keywords:

Meso-tetrakis(4-sulfonatophenyl) porphyrin  
TPPS  
Poly(vinylpyrrolidone)  
Isothermal titration calorimetry  
Dimer  
(Host + guest)

### ABSTRACT

Optical properties of porphyrins can be tuned through (polymer + porphyrin) (host + guest) binding in solution. This gives rise to the formation of supramolecular structures. In this paper, the formation, thermodynamic stability and spectroscopic properties of (polymer + porphyrin) supramolecular structures and their competition with porphyrin self-association were investigated by both isothermal titration calorimetry (ITC) and absorption spectroscopy. Specifically, reaction enthalpies and equilibrium constants were measured for meso-tetrakis(4-sulfonatophenyl) porphyrin (TPPS) self-association and TPPS binding to the polymer poly(vinylpyrrolidone) (PVP, 40 kg/mol) in aqueous solutions at pH 7 and three different temperatures (12, 25 and 37 °C). ITC, compared to spectroscopic techniques, provides two independent means to determine reaction enthalpies: direct measurements and Van't Hoff plot. This was used as a criterion to assess that (1) self-association of TPPS is limited to the formation of dimers and (2) TPPS binds to PVP in its monomeric state only. The formation of TPPS dimers and (PVP + TPPS) supramolecular structures are both enthalpically driven. However, (polymer + porphyrin) binding was found to be entropically favored compared to dimerization. Furthermore, the reaction enthalpies of these two processes significantly depend on temperature. This behavior was attributed to hydrophobic interactions. Finally, the limiting absorption spectra of monomeric, dimeric and polymer-bound states of TPPS were extracted from our spectroscopic measurements combined with the thermodynamic parameters obtained by ITC. The observed spectral shifts indicate that the two hydrogens in the central porphyrin are involved in (PVP + TPPS) binding. This work provides valuable information on thermodynamic stability of (polymer + porphyrin) supramolecular nanostructures and the general understanding of complex competing associative processes in solution.

© 2014 Elsevier Ltd. All rights reserved.

### 1. Introduction

Porphyrins are tetrapyrrolic macrocycles known for their interesting spectroscopic properties [1,2], supramolecular polymeric structures (e.g. J and H aggregates) [1,3] and catalytic applications [1,4]. In relation to spectroscopy, porphyrins display very strong absorption around (400 to 430) nm (Soret band) and relatively weaker absorption around (500 to 650) nm (Q bands) [2,5,6]. Excited singlet porphyrins show interesting photophysical properties leading to storage of energy and its transfer to their surroundings [7]. These properties are very valuable for applications in photodynamic therapy [7–10] and photoelectrical devices [11,12].

The formation of supramolecular structures of porphyrins in solution [13–20] have been mainly investigated by examining

the red shift (J aggregates, edge-to-edge stacking) and blue shift (H aggregates, face-to-face stacking) of their absorption spectra [14–18]. However, supramolecular structures with their own spectroscopic properties can be also obtained by introducing polymers that can bind porphyrins. These mesoscopic materials can find applications in nanotechnology, catalysis, medicine and separation technologies. However, (polymer + porphyrin) binding competes with porphyrin self-association in solution, and accurate thermodynamic studies are critical for the characterization of the thermodynamic stability of related supramolecular structures. Here, spectroscopic techniques alone provide a limited understanding on the energetics of these complicated associative processes.

In this paper, isothermal titration calorimetry (ITC) is successfully used for characterizing both (polymer + porphyrin) binding and porphyrin self-association for meso-tetrakis(4-sulfonatophenyl) porphyrin (TPPS) in water at pH 7.0 [14–21]. UV/visible spectra were also obtained in similar experimental conditions and discussed in relation to our ITC results.

\* Corresponding author. Tel.: +1 (817) 257 6215; fax: +1 (817) 257 5851.  
E-mail address: [O.Annunziata@tcu.edu](mailto:O.Annunziata@tcu.edu) (O. Annunziata).

Compared to spectroscopic techniques, ITC has the advantage of providing both the equilibrium constant (or standard reaction Gibbs free energy) of a reversible chemical reaction and the corresponding reaction enthalpy [22,23]. Note that reaction enthalpies can be also obtained by determining equilibrium constants from spectroscopic measurements as a function of temperature (Van't Hoff plot). Consequently, if equilibrium constants are measured by ITC as a function of temperature, two independent means of determining the same reaction enthalpy become available from ITC. This unique feature is very important for assessing the accuracy of the binding models chosen to describe complex chemical equilibria. Furthermore, reaction enthalpies extracted from individual ITC measurements as a function of temperature offers a precise way to determine the reaction heat capacity. This thermodynamic parameter is known to be important for evaluating the contribution of hydrophobic interactions to binding processes in aqueous solutions [22]. To our knowledge, there is only one qualitative ITC study related to TPPS binding to ferric myoglobin, [24] and there are only few ITC investigations on porphyrins in general [25,26].

TPPS has four negatively charged sulfonate groups that compensate for the hydrophobicity of the aromatic tetrapyrrolic system and the attached four phenyl groups. The amphiphilic properties of this porphyrin lead to complex self-association behavior in aqueous solutions, depending on physicochemical parameters such as concentration, temperature, ionic strength and pH [14–19,21,27]. Furthermore, additives such as polymers [20,27–30] and surfactants [31–33] may non-covalently bind to porphyrins thereby providing another way to modulate their aggregation state and solubility in solution. Two  $pK_a$  points near pH 5 can be associated with TPPS [34]. These characterize the effect of pH on the protonation state of the two pyrrole nitrogens in the central porphyrin ring. Thus, TPPS displays a net charge of  $-4$  at  $pH \approx 7$  (free base state) and  $-2$  at  $pH \approx 3$  (diacid state). The reduction of electrostatic repulsion at low pH facilitates self-association of the diacid state compared to that of the free base porphyrin at neutral and high pH [17]. The spectroscopic behavior of TPPS in aqueous solutions has been utilized to characterize TPPS self-association in aqueous solution as a function of pH [14–17]. This process may be described by employing a dimerization model at neutral and high pH, while the self-association occurring at low pH is more complex and normally involves the formation of large J-aggregates.

In this paper, poly(vinylpyrrolidone) (PVP) is used to obtain (PVP + TPPS) supramolecular structures at physiological pH. Specifically, we provide an accurate thermodynamic characterization of TPPS self-association, (PVP + TPPS) binding and related stoichiometry. PVP is a hydrophilic neutral polymer extensively employed in pharmacological applications [35]. For example, PVP is used as a binder in tablet formulations and as a solubilizing agent for active ingredients. There is one spectroscopic study [30] reporting on (PVP + TPPS) binding. However, this investigation was limited to acidic pHs and neglects the very important contribution of TPPS self-association. These (PVP + TPPS) binding studies will also provide the basis for investigating, by ITC, the more complex self-association behavior of TPPS at low pH. Here, PVP can be employed to dissociate individual units from porphyrin aggregates, thereby probing their binding energy.

## 2. Experimental section

### 2.1. Materials

5,10,15,20-Tetraphenyl-21H,23H-porphine-*p,p',p'',p'''*-tetrasulfonic acid tetrasodium hydrate (TPPS) was purchased from Sigma-Aldrich, and used as supplied, without further purification.

(TPPS + water) stock solutions with a composition of  $\approx 1\%$  (w/w) were prepared by weight. Poly(vinylpyrrolidone) (PVP) with nominal molecular weight of  $40 \text{ kg} \cdot \text{mol}^{-1}$  was purchased from Sigma-Aldrich and used without further purification. Complete specification of materials is listed in table 1. Deionized water was passed through a four-stage Millipore filter system to provide higher purity water for all the experiments. (PVP + water) stock solutions with a composition of  $\approx 10\%$  (w/w) were prepared by weight. The solutions for ITC and spectroscopic measurements were gravimetrically prepared by mixing known amounts of TPPS and/or PVP stock solutions with water and buffer. A 0.10-M, pH 7.0 sodium phosphate buffer was also added so that the final phosphate concentration was 0.010 M. TPPS and PVP weight fractions were converted into the corresponding molar concentrations using the molecular weights of ( $1023$  and  $111.14$ )  $\text{kg} \cdot \text{mol}^{-1}$  for TPPS and PVP monomeric unit respectively and the solution specific volume calculated using the specific volumes of ( $0.78$  and  $0.999$ )  $\text{cm}^3 \cdot \text{g}^{-1}$  for PVP [36] and 0.010-M aqueous buffer respectively. The small contribution of TPPS to the solution specific volume was neglected.

### 2.2. Isothermal titration calorimetry

ITC measurements were performed using the MicroCal iTC200 System from GE Healthcare Life Sciences. All experiments were performed at  $T = (12, 25 \text{ and } 37)^\circ\text{C}$  and atmospheric pressure ( $\approx 0.99$  bar). For dissociation experiments, small aliquots ( $2.0 \mu\text{L}$ ) of a TPPS aqueous solution (titrant,  $3.69 \text{ mM}$ ) were sequentially injected ( $\approx 20$  injections) from a rotating syringe into the vigorously stirred sample cell (syringe rotation,  $1000 \text{ rpm}$ ) containing porphyrin-free 0.010-M buffer (titrand). The reaction cell volume is  $203.4 \mu\text{L}$  according to factory specifications. TPPS dilution into the cells leads to porphyrin disaggregation, which resulted in the isothermal absorption of heat from the surroundings. For (PVP + TPPS) binding experiments, small aliquots ( $2.0 \mu\text{L}$ ) of a PVP aqueous solution (titrant,  $91.0 \text{ mM}$ ) were sequentially injected into the ITC cell containing a TPPS aqueous solution (titrand,  $0.244 \text{ mM}$ ). The choice of PVP instead of TPPS as the titrant was imposed by the large contribution of TPPS dilution to the recorded heat (due to porphyrin dissociation). On the other hand, blank experiments, in which PVP solutions were injected into pure buffer, showed that the contribution of PVP dilution to the overall heat involved in the (PVP + TPPS) mixing process is very small.

Each injection corresponds to a peak on a plot showing the power required to maintain the sample and reference cells at the same temperature as a function of time. The differential heat associated with each injection is calculated as the area of the corresponding measured peak and normalized with respect to the titrant number of moles. The differential heat  $q^{(i)}$  associated with injection  $i$  is linked to the cumulative heat  $Q^{(i)}$  absorbed or released by the sample inside the stirred cell after injection  $i$  by applying

$$q^{(i)} = \left[ (V + v/2)(Q^{(i)}/V) - (V - v/2)(Q^{(i-1)}/V) \right] / (vC'_{\text{TITRANT}}), \quad (1)$$

where  $Q^{(0)} = 0$ ,  $V = 203.4 \mu\text{L}$  is the volume of sample cell,  $v = 2.0 \mu\text{L}$  is the volume of individual titrant injections and  $C'_{\text{TITRANT}}$  is the titrant concentration. The volumetric factors  $(V + v/2)/V = 1.005$  and  $(V - v/2)/V = 0.995$  represent small corrections taking into account that the titrant addition to the sample cell displaces a small fraction ( $v/V \approx 0.01$ ) of solution outside the stirred sample cell. Thus, the experimentally recorded differential heat corresponds to an overestimate of  $Q^{(i)}$  because a small contribution to heat will also come from the sample displaced outside the cell, and an underestimate of  $Q^{(i-1)}$  because this displaced sample contributed to the cumulative heat after injection  $i - 1$ . Thus  $Q^{(i-1)}$  does not represent the correct starting point for injection  $i$ . The two factors  $(V \pm v/2)/V$  represent the average between two

TABLE 1

The provenience and purity of the materials used.

Chemical name	Source	Mass fraction purity	Purification method
Tetrasodium tetraphenylporphyrinetetrasulfonate	Sigma-Aldrich	>0.99	None
Poly(vinylpyrrolidone), Molecular Weight, 40 kg · mol <sup>-1</sup>	Sigma-Aldrich	>0.99	None
Sodium phosphate dibasic dihydrate	Fisher Scientific	0.98 to 1.01	None
Sodium phosphate monobasic anhydrous	Fisher Scientific	0.98 to 1.03	None

limiting conditions:  $(V \pm \nu)/V$  (mixing occurring before sample displacement) and 1 (mixing occurring after sample displacement).

Theoretical binding models are then used to obtain mathematical expressions linking  $Q^{(i)}/V$  to the total concentrations of titrant,  $C_{\text{TITRANT}}^{(i)}$ , and titrand,  $C_{\text{TITRAND}}^{(i)}$ , inside the sample cell after injection  $i$ . These concentrations are calculated by applying

$$C_{\text{TITRANT}}^{(i)} = [i\nu/(V + i\nu/2)]C'_{\text{TITRANT}}, \quad (2)$$

$$C_{\text{TITRAND}}^{(i)} = [(V - i\nu/2)/(V + i\nu/2)]C'_{\text{TITRAND}}, \quad (3)$$

where  $C'_{\text{TITRAND}} = C_{\text{TITRAND}}^{(0)}$  is the initial concentration of titrand inside the sample cell. The volumetric factors that were already shown for  $q^{(i)}$  take into account concentration reductions due to the small sample displacement outside the cell. Specifically, equation (2) is the average between the following two limiting mass balances:  $(V + i\nu)C_{\text{TITRANT}}^{(i)} = i\nu C'_{\text{TITRANT}}$  (mixing occurring before sample displacement) and  $VC_{\text{TITRANT}}^{(i)} = i\nu C'_{\text{TITRANT}}$  (mixing occurring after sample displacement). Similarly, equation (3) is the average between the following two limiting mass balances:  $(V + i\nu)C_{\text{TITRAND}}^{(i)} = VC'_{\text{TITRAND}}$  (mixing occurring before sample displacement) and  $VC_{\text{TITRAND}}^{(i)} = (V - i\nu)C'_{\text{TITRAND}}$  (mixing occurring after sample displacement).

The mathematical expressions shown for  $Q^{(i)}/V$  in Section 3 were then inserted in equation (1). Note that the superscript “(i)” for  $Q^{(i)}/V$  will be omitted in Section 3 since  $Q^{(i)}/V$  is a continuum function of the sample composition. The method of least squares is applied to the differential heat  $q^{(i)}$ . Specifically, the summation taken over  $N$  experimental points,  $\sum_{i=1}^N (q_{\text{exp}}^{(i)} - q_{\text{cal}}^{(i)})^2$ , is minimized using MATLAB, where  $q_{\text{exp}}^{(i)}$  is the experimental differential heat,  $q_{\text{cal}}^{(i)}$  represents the employed mathematical model, which is a function of a set of  $M$  parameters  $a_k$  (i.e., standard reaction enthalpy, equilibrium constant and number of binding sites);  $M = 2$  for self-association models and  $M = 3$  for (host + guest) association models. Standard deviations associated with the parameters extracted from the method of least squares were evaluated in the following way. For each of the  $N$  experimental points, the  $M$  partial derivatives,  $\partial q^{(i)}/\partial a_k$ , where numerically evaluated at the determined values of  $a_k$ . This gives a  $N \times M$  matrix here denoted as  $A$ . The  $M \times M$  (variance + covariance) matrix,  $S \equiv (A'A)^{-1}\sigma^2$ , was then calculated, where  $A'$  is the transpose of  $A$ , and  $\sigma^2 = \sum_{i=1}^N (q_{\text{exp}}^{(i)} - q_{\text{cal}}^{(i)})^2 / (N - M)$ . [37] The standard deviations of the  $M$  fitting parameters were taken as the square root of the  $M$  diagonal elements of  $S$ .

### 2.3. Absorption spectra

Absorption spectra were obtained at room temperature ( $\approx 21$  to  $22$  °C) and atmospheric pressure ( $\approx 0.99$  bar) with a Beckman DU 800 using two cuvettes with path length of ( $l = 1$  and  $l = 0.1$ ) cm for experiments in the wavelength range: (500 to 700) nm ( $Q$  bands) and in the wavelength range: (400 to 450) nm (Soret band) respectively. The obtained results were reported as normalized

absorption spectra by calculating the molar absorption coefficient:  $\varepsilon = \text{Abs}/(lC)$ , where  $\text{Abs}$  is the corresponding sample absorbance and  $C$  is the corresponding TPPS concentration.

## 3. Results and discussion

### 3.1. TPPS self-association

In figure 1(A), we show differential-heat plots for our ITC dissociation experiments at  $T = (12, 25$  and  $37)$  °C. In all three cases, we obtain positive heat values consistent with dissociation being an endothermic process. Our data were examined using the dimerization model:  $L_2 = 2L$ , [37,38] where  $L$  and  $L_2$  denote the TPPS monomer and dimer respectively. Note that we will also apply the equal-constant self-association model [39] to TPPS. Thus, to discuss similarities and differences between these two models applied to our ITC data, we first review the dimerization model, while the other model will be examined at the end of this section. The cumulative heat for the dissociation TPPS dimers is given by

$$Q/V = ([L_2] - [L_2]_0)\Delta_d H_{\text{dim}}^0, \quad (4)$$

where  $[L_2]$  is dimer concentration in the ITC cell,  $[L_2]_0$  is the hypothetical concentration of dimers in the sample cell calculated by assuming that all dimers transferred from the titrant solution do not dissociate, and  $\Delta_d H_{\text{dim}}^0$  is the standard enthalpy for dimer dissociation. Note that the value of  $Q/V$  is directly related to the dimer concentration because there is one binding interaction per dimer molecule. The dimer concentration is then related to the monomer concentration,  $[L]$ , according the mass-action law:

$$\alpha_{\text{dim}} = \frac{[L]^2}{[L_2]}, \quad (5)$$

where  $\alpha_{\text{dim}}$  is the dissociation equilibrium constant. The monomer concentration is related to the known total concentration of TPPS,  $C_L$ , by the mass balance:

$$\frac{C_L}{[L]} = 1 + 2 \frac{[L]}{\alpha_{\text{dim}}}. \quad (6)$$

For this model, the following analytical expression for  $[L]$  can be obtained: [38,39]

$$[L] = \frac{\alpha_{\text{dim}}}{4} \left( \left( 1 + \frac{8C_L}{\alpha_{\text{dim}}} \right)^{1/2} - 1 \right). \quad (7)$$

Equations (5) and (7) are then used to obtain an expression for  $[L_2]$  in equation (4). The corresponding expression of  $[L_2]_0$  is obtained by first calculating the dimer concentration in the titrant solution and then applying the dilution factor (see equation (2)).

In table 2, we report the determined values of  $\alpha_{\text{dim}}$  and  $\Delta_d H_{\text{dim}}^0$ . Note that  $\alpha_{\text{dim}}$  increases with temperature. This is qualitatively consistent with dissociation being an endothermic process. The corresponding values of standard Gibbs free energy and entropy were then calculated using  $\Delta_d G_{\text{dim}}^0 = -RT \ln \alpha_{\text{dim}}$  and  $\Delta_d S_{\text{dim}}^0 = (\Delta_d H_{\text{dim}}^0 - \Delta_d G_{\text{dim}}^0)/T$  respectively, where  $R$  is the ideal-gas constant and  $T$  the absolute temperature. As shown in table 2

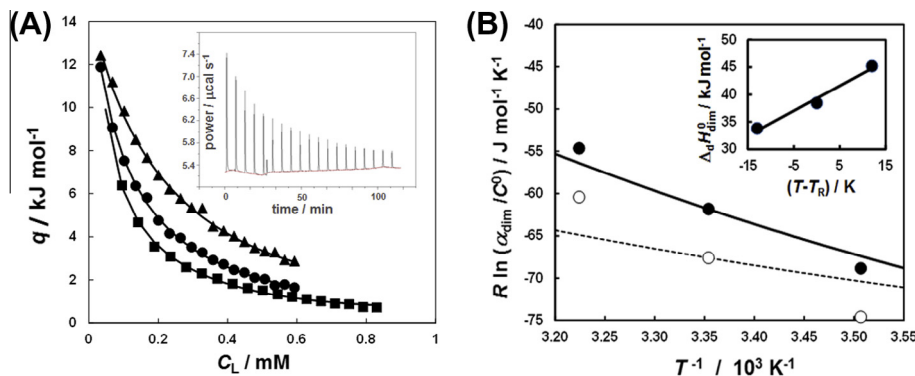


**FIGURE 1.** (A) Differential heat,  $q$ , associated with consecutive injections of titrant solution (TPPS, 3.69 mM; sodium phosphate buffer, 10 mM, pH 7.0) into the titrand solution (sodium phosphate buffer, 10 mM, pH 7.0) as a function of TPPS concentration after injection in the ITC cell,  $C_L$ , at  $T = 12^\circ\text{C}$  (squares),  $T = 25^\circ\text{C}$  (circles) and  $T = 37^\circ\text{C}$  (triangles). The inset shows a representative plot of power as a function of time for the titration at  $T = 25^\circ\text{C}$ . (B) Van't Hoff plot for the TPPS dimer dissociation constant,  $\alpha_{\text{dim}}$ , as a function of temperature (solid circles). The solid curve describes the behavior of  $\alpha_{\text{dim}}$  predicted starting from its experimental value at  $T = 25^\circ\text{C}$  and the corresponding reaction enthalpy and heat capacity values extracted from ITC experiments. The Van't Hoff plot for the dissociation constants obtained by applying the equal-constant self-association model (open circles) and the predicted behavior (dashed curve) from the corresponding reaction enthalpy and heat capacity values is also included.  $C^\ominus \equiv 1 \text{ M}$  is the standard concentration and  $T_R \equiv 25^\circ\text{C}$  is the chosen reference temperature. The inset shows the standard dissociation enthalpy for TPPS dimers as a function of temperature.

**TABLE 2**  
Thermodynamic parameters associated with TPPS dimerization.

$T/\text{K}^a$	285.15	298.15	310.15
$\alpha_{\text{dim}}/\text{mM}$	$0.25 \pm 0.01^b$	$0.58 \pm 0.02$	$1.4 \pm 0.1$
$\Delta_d H_{\text{dim}}^0/\text{kJ} \cdot \text{mol}^{-1}$	$33.9 \pm 0.4$	$38.5 \pm 0.4$	$45.2 \pm 0.4$
$\Delta_d C_{\text{dim}}^0/\text{kJ} \cdot \text{mol}^{-1}$	$19.6 \pm 0.08^c$	$18.5 \pm 0.08$	$16.9 \pm 0.17$
$\Delta_d S_{\text{dim}}^0/\text{J} \cdot \text{mol}^{-1} \cdot \text{K}^{-1}$	$50 \pm 1$	$67 \pm 1$	$91 \pm 1$
$\alpha_{\text{dim}}/\text{mM}$ (calc)	$0.300^d$		1.13

<sup>a</sup> Uncertainty:  $u(T) = \pm 0.00015 \text{ K}$  (temperature stability).

<sup>b</sup> Uncertainties:  $u(\alpha_{\text{dim}})$  and  $u(\Delta_d H_{\text{dim}}^0)$  are standard deviations from the method of least squares (see Section 2.2).

<sup>c</sup> Uncertainties:  $u(\Delta_d C_{\text{dim}}^0)$  and  $u(\Delta_d S_{\text{dim}}^0)$  were calculated from  $u(\Delta_d C_{\text{dim}}^0) = RT u(\alpha_{\text{dim}})/\alpha_{\text{dim}}$  and  $u(\Delta_d S_{\text{dim}}^0) = \left( u(\Delta_d H_{\text{dim}}^0)^2 + u(\Delta_d C_{\text{dim}}^0)^2 \right)^{1/2} / T$  respectively.

<sup>d</sup> Values calculated using  $R \ln \alpha_{\text{dim}} = \Delta_d S_{\text{dim},R}^0 - \Delta_d H_{\text{dim},R}^0/T - \Delta_d C_{p,\text{dim}}^0 \ln(1 - T_R/T) - \ln(T/T_R)$ .

and in the inset of figure 1(B),  $\Delta_d H_{\text{dim}}^0$  increases with temperature. Thus, the constant-pressure heat capacity of dissociation,  $\Delta_d C_{p,\text{dim}}^0 = (0.45 \pm 0.06) \text{ kJ} \cdot \text{mol}^{-1} \cdot \text{K}^{-1}$ , was determined by applying the method of least squares based on  $\Delta_d H_{\text{dim}}^0 = \Delta_d H_{\text{dim},R}^0 + \Delta_d C_{p,\text{dim}}^0 \cdot (T - T_R)$ , where  $T_R = 298.15 \text{ K}$  is our chosen reference temperature and  $\Delta_d H_{\text{dim},R}^0 = (39.3 \pm 0.6) \text{ kJ} \cdot \text{mol}^{-1}$  is its corresponding  $\Delta_d H_{\text{dim}}^0$  value extracted from the fit.

The dependence of the dissociation constant on temperature can be described using the following thermodynamic relation derived by assuming that  $\Delta_d C_{p,\text{dim}}^0$  is independent of temperature: [22]

$$R \ln \alpha_{\text{dim}} = \Delta_d S_{\text{dim},R}^0 - \frac{\Delta_d H_{\text{dim},R}^0}{T} - \Delta_d C_{p,\text{dim}}^0 \cdot \left( \frac{T - T_R}{T} - \ln \frac{T}{T_R} \right), \quad (8)$$

where  $\Delta_d S_{\text{dim},R}^0 = (70 \pm 3) \text{ J} \cdot \text{mol}^{-1} \cdot \text{K}^{-1}$  is the dissociation entropy value at  $T_R$  calculated from  $\Delta_d H_{\text{dim},R}^0$  and the value of  $\Delta_d C_{p,\text{dim}}^0$  at  $T = 298.15 \text{ K}$  in table 2. In figure 1(B), the experimental values of  $R \ln \alpha_{\text{dim}}$  are plotted together with the theoretical curve generated by using equation (8). The values of  $\alpha_{\text{dim}}$  calculated from equation (8) (see last row in table 2) exhibit an error lower than 20% compared to those directly obtained from ITC experiments. We believe that this is an acceptable discrepancy for experimental equilibrium constants.

Spectroscopy studies have shown that TPPS polymeric aggregates are formed through edge-to-edge stacking [14]. Specifically, to minimize electrostatic repulsion between two parallel porphyrins, a sulfonate group of a porphyrin interacts with the center of the other porphyrin. However, steric considerations indicate that higher-order linear oligomers can be also formed through edge-to-edge stacking. Thus, we have also examined our ITC dissociation experiments using the equal-constant self-association model, in which soluble reversible oligomers can also occur according to  $L_k = L_{k-1} + L$ , [39,40] with  $k = 2, 3, 4, \dots$ . Here, the dissociation constant,  $\alpha_{\text{olig}}$ , of a monomeric unit from an oligomer is independent of the degree of oligomerization: [39]

$$\alpha_{\text{olig}} = \frac{[L][L_{k-1}]}{[L_k]}, \quad \text{with } k = 2, 3, 4, \dots \quad (9)$$

This model is consistent with the hypothesis that stacking of a third porphyrin molecule can also occur on one of the two dimer sides, leading to the formation of linear oligomers. The cumulative heat for the dissociation of TPPS oligomers is given by

$$Q/V = \left( \sum_{k=2} (k-1)[L_k] - \sum_{k=2} (k-1)[L_k]_0 \right) \Delta_d H_{\text{olig}}^0, \quad (10)$$

where  $[L_k]$  is the concentration of oligomer  $k$  in the sample cell,  $[L_k]_0$  is the corresponding hypothetical concentration in the sample cell calculated by assuming that all oligomers transferred from the titrant solution do not dissociate, and  $\Delta_d H_{\text{olig}}^0$  is the standard enthalpy for the dissociation of a monomer unit from the oligomers, also assumed to be independent of the degree of oligomerization. Note that the  $(k-1)$  factor in equation (10) implies that there are  $(k-1)$  binding interactions in the linear oligomer  $L_k$  and neglects the formation of cyclic assemblies.

The monomer concentration is related to  $C_L$ , by the mass balance:  $C_L = [L_k] + \sum_{k=2} k[L_k]$ . The second term on the right side of the mass balance can be rewritten as a geometric series, leading to the following expression:

$$\frac{C_L}{[L]} = \left( 1 - \frac{[L]}{\alpha_{\text{olig}}} \right)^{-2}. \quad (11)$$

For this model, the following analytical expression for  $[L]$  can be obtained [39,40]:

$$[L] = \frac{\alpha_{\text{olig}}^2}{2C_L} \left( 1 + \frac{2C_L}{\alpha_{\text{olig}}} - \left( 1 + \frac{4C_L}{\alpha_{\text{olig}}} \right)^{1/2} \right). \quad (12)$$

Equations (9) and (12) can be then used to obtain an expression for  $[L_k]$  in equation (10).

We are now in position to compare the two models applied to ITC data. Note that the mathematical structure of equation (10) is the same as that of equation (4). This can be appreciated by comparing the obtained expressions for  $[L_2]$  and  $\sum_{k=2} (k-1)[L_k]$  reported below:

$$[L_2] = \frac{[L]^2}{\alpha_{\text{dim}}} = \frac{\alpha_{\text{dim}}}{8} \left( 1 + \frac{4C_L}{\alpha_{\text{dim}}} - \left( 1 + \frac{8C_L}{\alpha_{\text{dim}}} \right)^{1/2} \right), \quad (13)$$

$$\sum_{k=2} (k-1)[L_k] = \frac{\alpha_{\text{olig}} [L]^2}{(\alpha_{\text{olig}} - [L])^2} = \frac{\alpha_{\text{olig}}}{2} \left( 1 + \frac{2C_L}{\alpha_{\text{olig}}} - \left( 1 + \frac{4C_L}{\alpha_{\text{olig}}} \right)^{1/2} \right). \quad (14)$$

The comparison of equation (13) with equation (14) allows us to deduce that these two equations are identical if  $\alpha_{\text{olig}} = \alpha_{\text{dim}}/2$  and  $\Delta_d H_{\text{olig}}^0 = \Delta_d H_{\text{dim}}^0/2$ . Since reaction enthalpy is linked to the equilibrium-constant logarithm, we can appreciate that the discrepancy between the enthalpy values directly extracted from the ITC experiments with those obtained from the Van't Hoff plot represents a decisive criterion in assessing the relative accuracy of the two proposed models.

In figure 1(B), we also include the experimental values of  $R \ln \alpha_{\text{olig}}$  together with the corresponding theoretical curve based on Van't Hoff equation. The relatively large deviation between experimental values and calculated curve shows how ITC data can be used to deduce that dimerization is the more accurate model in this case. Here, electrostatic repulsions play a critical role in hindering the formation of highly-charged porphyrin oligomers.

The value of  $\Delta_d H_{\text{dim,R}}^0$  is comparable with those extracted from spectroscopic experiments [41] and indicates that porphyrin dimerization is an enthalpically driven process. However ITC experiments have also allowed us to characterize the dependence of  $\Delta_d H_{\text{dim,R}}^0$  on temperature (see inset in figure 1(B)). An increase of  $\Delta_d H_{\text{dim,R}}^0$  with temperature is consistent with the presence of hydrophobic interactions. For instance, it has been estimated that the contribution of one water molecule to the reaction heat capacity in the ice-like cage around hydrophobic moieties of biomolecules is about  $13 \text{ J} \cdot \text{mol}^{-1} \cdot \text{K}^{-1}$  [42]. Our value of  $\Delta_d C_{p,\text{dim}}^0$  is about 30-fold higher, thereby indicating significant hydrophobic interactions to the dimer dissociation.

Contrary to  $\Delta_d H_{\text{dim,R}}^0$  and  $\Delta_d C_{p,\text{dim}}^0$ , the value of  $\Delta_d S_{\text{dim,R}}^0$  is of more difficult interpretation. Indeed, even the sign of  $\Delta_d S_{\text{dim,R}}^0$  will depend on the choice of the standard state due to the effect of solution volume on the translational entropy of individual solute particles. Assuming that the solvent can be treated as a continuum, the standard translational entropy of  $160 \text{ J} \cdot \text{mol}^{-1} \cdot \text{K}^{-1}$  can be calculated for dissociative processes using the Sackur–Tetrode equation [43]. This value can be compared to the experimental  $\Delta_d S_{\text{dim,R}}^0$ . Note that the rotational entropy, which is independent of the choice of the standard state, will also positively contribute to the net reaction entropy. On the other hand, effects related to the solvent molecular structure such as excluded-volume and hydrophobic effects are expected to negatively contribute to  $\Delta_d S_{\text{dim,R}}^0$ . That the experimental values of reaction entropy in table 2 are significantly lower than  $160 \text{ J} \cdot \text{mol}^{-1} \cdot \text{K}^{-1}$  is also consistent with the presence of significant hydrophobic interactions.

### 3.2. (PVP + TPPS) supramolecular structures

In figure 2(A), we show differential-heat plots for our ITC (polymer + porphyrin) binding experiments at  $T = (12, 25 \text{ and } 37)^\circ\text{C}$ , demonstrating the formation of (polymer + porphyrin)

supramolecular structures. In all three cases, we obtain negative heat values consistent with binding being an exothermic process. Our data were examined using the Scatchard model based on equivalent and independent sites:  $PL_k = PL_{k-1} + L$  [38] with  $k = 1, 2, 3, \dots, n$ , where P denotes PVP and  $n$  is the total number of sites on the host polymer. Note that this reaction scheme assumes that only TPPS monomeric units bind to PVP. This assumption will be further discussed at the end of this section. The cumulative heat for (polymer + porphyrin) binding is given by

$$Q/V = ([L_2] - [L_2]_0) \Delta_d H_{\text{dim}}^0 - \nu C_p \Delta_d H_{\text{PL}}^0. \quad (15)$$

Here  $[L_2]_0$  is the hypothetical concentration of dimers in the sample cell calculated by assuming that all dimers in the titrand solution do not dissociate after the addition of polymer, and  $\nu$  is the number of porphyrin molecules bound per polymer unit. According to the Scatchard model, this is linked to the free monomer concentration,  $[L]$ , by

$$\nu = \frac{n[L]}{K + [L]}. \quad (16)$$

The thermodynamic parameters  $\Delta_d H_{\text{PL}}^0$  in equation (15) and  $K$  in equation (16) are the standard enthalpy and equilibrium constant for (polymer + porphyrin) dissociation respectively. The total polymer concentration,  $C_p$ , is defined with respect to PVP monomer molecular weight. This implies that formally  $n$  is a fractional number if the polymer binding site consists of several PVP monomers; i.e., the number of monomers involved in a binding site is  $1/n$ . Equation (15) shows that the observed  $Q/V$  has to take into account not only the heat associated with (polymer + porphyrin) binding (second term of RHS) but also that contribution coming from dimer dissociation (first term of RHS), which is promoted by (porphyrin + polymer) binding.

The free monomer concentration,  $[L]$ , is related to  $C_L$ , by the mass balance:  $C_L = [L] + 2[L_2] + \nu C_p$ , which can be rewritten in the following way:

$$\frac{C_L}{[L]} = 1 + 2 \frac{[L]}{\alpha_{\text{dim}}} + \frac{n C_p}{K + [L]}. \quad (17)$$

Equation (17) can be rearranged as a cubic equation with respect to  $[L]$ , and its three roots were numerically calculated as a function of  $\alpha_{\text{dim}}$ ,  $K$  and  $n$  using MATLAB. Clearly, the free monomer concentration must be low enough so that all concentrations satisfying the mass balance are positive. Thus, the value of  $[L]$  was taken as the lowest real positive root. The method of least squares was then applied to equation (15) by using the values of  $\Delta_d H_{\text{dim}}^0$  and  $\alpha_{\text{dim}}$  from table 2 and by calculating the deviation between experimental  $Q/V$  and that calculated from equation (15) after systematically varying the values of  $\Delta_d H_{\text{PL}}^0$ ,  $K$  and  $n$ . In table 3, we report the determined values of  $\Delta_d H_{\text{PL}}^0$ ,  $K$  and  $n$ . Note that  $K$  increases with temperature, consistent with (polymer + porphyrin) dissociation being an endothermic process. These values can be used to deduce that substantial formation of (PVP + TPPS) supramolecular structures is obtained when the obtained when the porphyrin concentration in the surrounding aqueous medium is of the order of  $10 \mu\text{M}$  or higher. From the obtained values of  $n$ , we deduce that there are about 20 PVP monomers involved in the binding of one TPPS molecule. This implies that the molecular weight of the saturated (PVP + TPPS) supramolecular structure is  $\approx 50\%$  larger than that of the polymeric scaffold. Note that  $1/n$  was found to slightly increase with temperature. This behavior can be related to the effect of temperature on solvent quality. Specifically, according to thermodynamic and viscosity experiments, [44] the hydrodynamic volume of PVP chains decreases as temperature increases. As temperature increases, polymer chains contract making PVP monomers less accessible to other molecules. Hence, more PVP monomers contribute to one binding site.

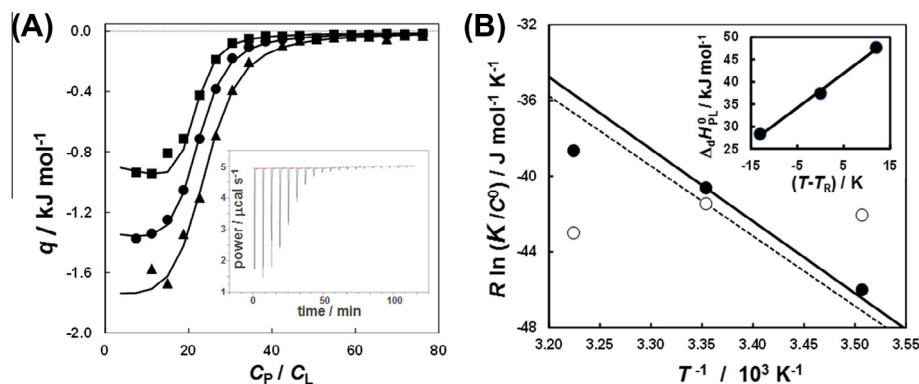


**FIGURE 2.** (A) Differential heat,  $q$ , associated with consecutive injections of titrant solution (PVP, 91.0 mM; sodium phosphate buffer, 10 mM, pH 7.0) into the titrand solution (TPPS, 0.244 mM; sodium phosphate buffer, 10 mM, pH 7.0) as a function of the PVP to TPPS concentration ratio after injection,  $C_P/C_L$ , at  $T = 12^\circ\text{C}$  (squares),  $T = 25^\circ\text{C}$  (circles) and  $T = 37^\circ\text{C}$  (triangles). The inset shows a representative plot of power as a function of time for the titration at  $T = 25^\circ\text{C}$ . (B) Van't Hoff plot for the (PVP + TPPS) dissociation constant,  $K$ , as a function of temperature (solid circles), obtained by assuming that TPPS binds to PVP in its monomeric state only. The solid curve describes the behavior of  $K$  predicted from its experimental value at  $T = 25^\circ\text{C}$  and the corresponding reaction enthalpy and heat capacity values extracted from ITC experiments. The Van't Hoff plot for the (PVP + TPPS) dissociation constants (open circles), obtained by assuming that TPPS dimers bind to PVP in the same way as TPPS monomers, and the predicted behavior (dashed curve) from the corresponding reaction enthalpy and heat capacity values is also included.  $C^\ominus \equiv 1\text{ M}$  is the standard concentration and  $T_R \equiv 25^\circ\text{C}$  is the chosen reference temperature. The inset shows the standard dissociation enthalpy for (PVP + TPPS) complexes as a function of temperature.

**TABLE 3**  
Thermodynamic parameters associated with (PVP + TPPS) binding.

$T/\text{K}^a$	285.15	298.15	310.15
$1/n$	$18.7 \pm 0.2^b$	$19.6 \pm 0.2$	$21.8 \pm 0.4$
$K/\mu\text{M}$	$3.9 \pm 0.5$	$7.5 \pm 0.5$	$9.5 \pm 1.5$
$\Delta_d H_{\text{PL}}^0/\text{kJ} \cdot \text{mol}^{-1}$	$28.5 \pm 0.3$	$37.4 \pm 0.3$	$47.7 \pm 1.0$
$\Delta_d G_{\text{PL}}^0/\text{kJ} \cdot \text{mol}^{-1}$	$29.5 \pm 0.3^c$	$29.3 \pm 0.2$	$29.8 \pm 0.4$
$\Delta_d S_{\text{PL}}^0/\text{J} \cdot \text{mol}^{-1} \cdot \text{K}^{-1}$	$-4 \pm 2$	$27 \pm 1$	$58 \pm 4$
$K/\mu\text{M}$ (calc)	$3.73^d$		13.6

<sup>a</sup> Uncertainty:  $u(T) = \pm 0.00015\text{ K}$  (temperature stability).

<sup>b</sup> Uncertainties:  $u(1/n)$ ,  $u(K)$  and  $u(\Delta_d H_{\text{PL}}^0)$  are standard deviations from the method of least squares (see Section 2.2).

<sup>c</sup> Uncertainties:  $u(\Delta_d G_{\text{PL}}^0)$  and  $u(\Delta_d S_{\text{PL}}^0)$  were calculated from  $u(\Delta_d G_{\text{PL}}^0) = RT u(K)/K$  and  $u(\Delta_d S_{\text{PL}}^0) = \left( u(\Delta_d H_{\text{PL}}^0)^2 + u(\Delta_d G_{\text{PL}}^0)^2 \right)^{1/2} / T$  respectively.

<sup>d</sup> Values calculated using  $R \ln K = \Delta_d S_{\text{PL,R}}^0 - \Delta_d H_{\text{PL,R}}^0/T - \Delta_d C_{p,\text{PL}}^0 [(1 - T_R/T) - \ln(T/T_R)]$ .

We now compare the thermodynamic strength of (PVP + TPPS) binding with that of TPPS dimerization. Note that the values of  $\Delta_d H_{\text{PL}}^0$  were found to be comparable with those of  $\Delta_d H_{\text{dim}}^0$ , while the values of  $K$  were found to be two order of magnitude smaller than those of  $\alpha_{\text{dim}}$ . This implies that (polymer + porphyrin) binding is stronger than porphyrin dimerization due to entropic effects. The corresponding values of standard Gibbs free energy and entropy, calculated using  $\Delta_d G_{\text{PL}}^0 = -RT \ln K$  and  $\Delta_d S_{\text{PL}}^0 = (\Delta_d H_{\text{PL}}^0 - \Delta_d G_{\text{PL}}^0)/T$  respectively, are also reported in table 3.

As shown in table 3 and in the inset of figure 2(B),  $\Delta_d H_{\text{PL}}^0$  increases with temperature. Thus, the constant-pressure heat capacity of dissociation,  $\Delta_d C_{p,\text{PL}}^0 = (0.77 \pm 0.04)\text{ kJ} \cdot \text{mol}^{-1} \cdot \text{K}^{-1}$ , was determined by applying the method of least squares based on  $\Delta_d H_{\text{PL}}^0 = \Delta_d H_{\text{PL,R}}^0 + \Delta_d C_{p,\text{PL}}^0 \cdot (T - T_R)$ , where  $\Delta_d H_{\text{PL,R}}^0 = (38.1 \pm 0.5)\text{ kJ} \cdot \text{mol}^{-1}$  is its corresponding  $\Delta_d H_{\text{PL}}^0$  value extracted from the fit. The dependence of the dissociation constant on temperature can be described as previously shown for porphyrin dimerization (see equation (8)). The standard dissociation entropy at  $T_R$  was calculated to be  $\Delta_d S_{\text{PL,R}}^0 = (30 \pm 2)\text{ J} \cdot \text{mol}^{-1} \cdot \text{K}^{-1}$  from  $\Delta_d H_{\text{PL,R}}^0$  and the value of  $\Delta_d G_{\text{PL}}^0$  at  $T = 298.15\text{ K}$  in table 3. The value of  $\Delta_d C_{p,\text{PL}}^0$  was found to be about 60% higher than that of  $\Delta_d C_{p,\text{dim}}^0$ . This indicates that more

significant hydrophobic interactions occur in (polymer + porphyrin) binding than in (porphyrin + porphyrin) dimerization. This is also consistent with  $\Delta_d S_{\text{PL,R}}^0$  being lower than  $\Delta_d S_{\text{dim,R}}^0$ . A large contribution of hydrophobic interaction in the case of (polymer + porphyrin) binding is consistent with both sides of a porphyrin molecule being involved in the interaction with the polymer chain. On the other hand, only one side per porphyrin is involved in the formation of a dimer.

Consideration on molecular sizes can be used to assess that the estimated lengths of the PVP binding site and porphyrin molecule are consistent with PVP chains interacting with both sides of TPPS. Specifically, we can estimate that the binding segment of PVP is  $\approx 6\text{ nm}$  based on the assumption that one PVP monomer contributes  $\approx 0.3\text{ nm}$  to the chain length and that there are about 20 PVP units contributing to a binding site. On the other hand, the diameter of TPPS, including the four peripheral groups, can be estimated to be  $\approx 2\text{ nm}$  [45]. Thus, the estimated lengths of the binding site and porphyrin are consistent with PVP chains interacting with both sides of TPPS.

In figure 2(B), the experimental values of  $R \ln K$  are plotted together with the theoretical curve generated by using the Van't Hoff equation. The corresponding calculated values of  $K$  (see last row in table 3) exhibit an error of 5% compared to the experimental value at  $T = 12^\circ\text{C}$  and 40% compared to the experimental value at  $T = 37^\circ\text{C}$ . These are acceptable discrepancies considering system relative complexity due to the presence of two binding processes. Note that an error of 40% in  $K$  corresponds to an error of  $1\text{ kJ} \cdot \text{mol}^{-1}$  in  $\Delta_d G_{\text{PL}}^0$ . This error remains comparable with the typical errors of  $\Delta_d H_{\text{PL}}^0$  data extracted by ITC.

For comparison, we have also examined our ITC binding experiments by assuming that both monomers and dimers equally bind to the polymer sites. The only modification to the previous model is that equation (16) is replaced by

$$v = \frac{n([L] + [L_2])}{K + ([L] + [L_2])}, \quad (18)$$

where  $L$  and  $L_2$  are treated as two distinct competing ligands with same binding properties. By following the same approach applied to equation (15), the extracted values of  $\Delta_d H_{\text{PL}}^0$  and  $n$  were found to be slightly different ( $\approx 5\%$ ) from those reported in table 3. However, the corresponding  $K$  values, which are shown in figure 2(B), were found to be virtually independent of temperature contrary

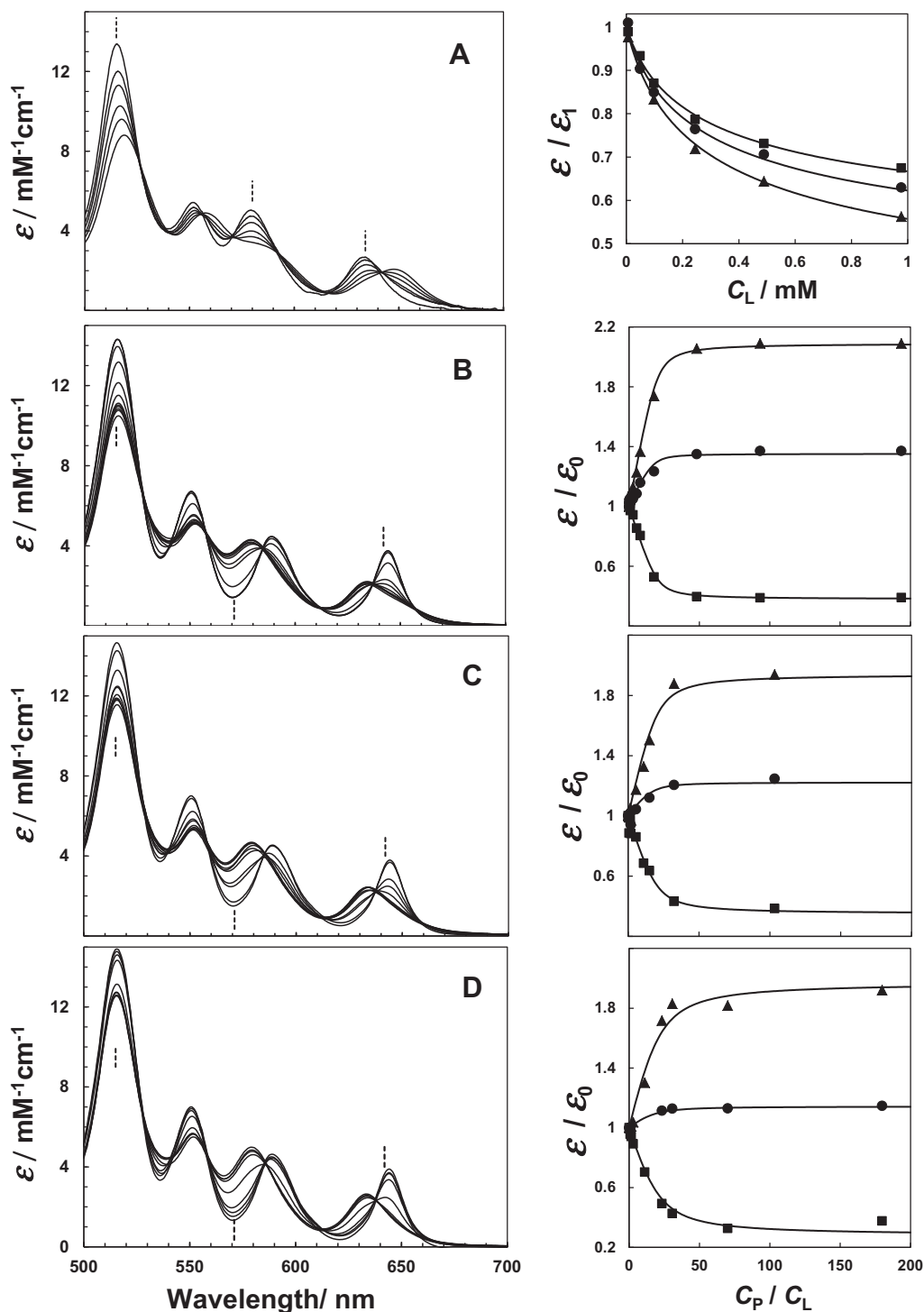


**FIGURE 3.** Normalized absorption spectra (extinction coefficient,  $\varepsilon$ ) showing the four Q bands of TPPS in sodium phosphate buffer, 10 mM, pH 7.0, 22.5 °C. (A) Spectra obtained at several TPPS concentrations,  $C_L$  in the absence of PVP. The dashed vertical bars identify three chosen wavelengths: (515, 580 and 634) nm. The effect of  $C_L$  on  $\varepsilon$  is described by the graphs on the right side showing the ratio,  $\varepsilon/\varepsilon_1$ , as a function of  $C_L$  at 515 nm (circles), 580 nm (squares) and 634 nm (triangles). The infinite-dilution values of the  $\varepsilon_1 = (13.3, 5.07 \text{ and } 2.75) \text{ mM}^{-1} \cdot \text{cm}^{-1}$  at (515, 580 and 634) nm were determined by applying the method of least squares with  $\alpha_{\text{dim}} = 0.54 \text{ mM}$ . The corresponding determined values of  $\varepsilon_2/\varepsilon_1$  were 0.37, 0.44 and 0.26 respectively. (B)–(D) Spectra obtained at several PVP concentrations,  $C_P$ , for three constant TPPS concentrations: 93.6  $\mu\text{M}$  (B), 47.9  $\mu\text{M}$  (C) and 23.2  $\mu\text{M}$  (D). The dashed vertical bars identify three chosen wavelengths: (515, 571 and 642) nm. The effect of the molar ratio,  $C_P/C_L$ , on  $\varepsilon$  is described by the corresponding graphs on the right side showing the ratio,  $\varepsilon/\varepsilon_0$ , as a function of  $C_P/C_L$  at 515 nm (circles), 571 nm (squares) and 642 nm (triangles). The values of  $\varepsilon_{PL}/\varepsilon_1 = 1.17, 0.38 \text{ and } 2.09$  (B), 1.12, 0.35 and 1.94 (C), and 1.09, 0.28 and 1.97 (D) at (515, 571 and 642) nm were determined by applying the method of least squares with  $\alpha_{\text{dim}} = 0.54 \text{ mM}$ ,  $K = 6.1 \mu\text{M}$  and  $n = 0.051$ . The wavelengths (571 and 642) nm corresponds to two isosbestic points in figure 5(A) with  $\varepsilon_2 = \varepsilon_1 = (5.07 \text{ and } 2.75) \text{ mM}^{-1} \cdot \text{cm}^{-1}$  respectively.

to the prediction from Van't Hoff equation (see figure 2(B)). We therefore deduce that the model based on equation (16) represents a more accurate description of (PVP + TPPS) binding. That the

interaction of polymer with L is favored compared to that with  $L_2$  is also consistent with the idea that PVP chains interact with both sides of a porphyrin.

### 3.3. Absorption spectra

In figure 3, we show normalized absorption spectra in the visible wavelength range for TPPS (figure 3(A)) and (PVP + TPPS) aqueous solutions (figure 3(B)–(D)) taken at room temperature ( $22.5 \pm 0.5$  °C). In figure 3(A), we can see the characteristic four Q bands of free-base porphyrins. As TPPS concentration increases, these bands shift towards higher wavelengths as expected for a J-type aggregation. Clearly, the existence of several isosbestic points is consistent with presence of chemical equilibrium between two different porphyrin species, *i.e.*, monomer and dimer.

We can use the dimer dissociation constant determined by ITC to describe the behavior of TPPS absorption spectra. At a given wavelength, the observed extinction coefficient of TPPS,  $\varepsilon$ , can be expressed as the weighted average between that of the monomer,  $\varepsilon_1$ , and dimer,  $\varepsilon_2$ , according to

$$\varepsilon = \frac{[L]}{C_L} \varepsilon_1 + \frac{2[L_2]}{C_L} \varepsilon_2, \quad (19)$$

where  $\varepsilon_2$  is defined with respect to the monomer molecular weight. The concentrations [L] and [L<sub>2</sub>] can be calculated as a function of C<sub>L</sub> by using  $\alpha_{\text{dim}}$ . We have used  $\alpha_{\text{dim}} = 0.54$  mM, which was calculated at  $T = 22.5$  °C by linear interpolation of  $\ln \alpha_{\text{dim}}$  (data taken from table 2) as a function of  $1/T$ . The values of  $\varepsilon_1$  and  $\varepsilon_2$  (see figure 3(A) caption) were then determined by applying the method of least squares. The graph on the right side of figure 3(A) shows  $\varepsilon/\varepsilon_1$  as a function of C<sub>L</sub> at three chosen wavelengths (515, 580 and 634 nm). These wavelengths correspond to the largest observed variations in  $\varepsilon$ . This graph shows that the curvature of the  $\varepsilon/\varepsilon_1$  data is accurately described by our ITC thermodynamic parameters.

In figure 3(B)–(D), we show porphyrin spectra as a function of PVP concentration at three constant TPPS concentrations. Here, we can use both the dimerization and (PVP + TPPS) binding data determined by ITC to describe the behavior of TPPS absorption spectra. At a given wavelength, the observed extinction coefficient of TPPS,  $\varepsilon$ , can be expressed as the following weighted average:

$$\varepsilon = \varepsilon_1 \frac{[L]}{C_L} + \varepsilon_2 \frac{2[L_2]}{C_L} + \varepsilon_{\text{PL}} \frac{\nu C_P}{C_L}, \quad (20)$$

where  $\varepsilon_{\text{PL}}$  is extinction coefficient of bound TPPS. The values of [L], [L<sub>2</sub>] and  $\nu$  can be calculated as a function of C<sub>L</sub> provided that  $\alpha_{\text{dim}}$ ,  $K$  and  $n$  are known. We have used  $K = 6.1$   $\mu\text{M}$  and  $n = 0.051$  calculated at  $T = 22.5$  °C from the linear interpolation of  $\ln K$  and  $n$  (data taken from table 3) as a function of  $1/T$ . The values of  $\varepsilon_{\text{PL}}$  (see figure 3(B)–(D) caption) were then determined by applying the method of least squares. The graphs on the right side of figure 3(B)–(D) show  $\varepsilon/\varepsilon_0$  as a function of  $C_P/C_L$  at the three investigated TPPS concentrations. Here,  $\varepsilon_0$  is the corresponding value of  $\varepsilon$  at  $C_P = 0$ . As we can see on the right side of figure 3(B)–(D), our ITC thermodynamic parameters adequately describe the behavior of the  $\varepsilon/\varepsilon_0$  data at three chosen wavelengths. One of these three wavelengths (515 nm) was chosen to be the same as that in figure 3(A). The other two wavelengths correspond to two isosbestic points (571 and 642 nm) for the (monomer + dimer) equilibrium, *i.e.*,  $\varepsilon_1 = \varepsilon_2$  and show a significant variation in  $\varepsilon$  as PVP concentration increases. On the other hand, the other two wavelengths in figure 3(B) (580 and 634 nm) were not considered because the corresponding variations in  $\varepsilon$  were relatively small.

Our values of  $\alpha_{\text{dim}}$ ,  $K$  and  $n$  were also used to extract the limiting spectra for monomer, dimer and bound states of TPPS. These spectra, which are shown in figure 4, allow us to examine the relative positions of the four Q bands. The observed shift between the four Q bands of monomer and dimer is (0.04 to 0.05) eV (see inset in figure 4). In the case of bound TPPS, the two Q<sub>x</sub> bands displays an intermediate location with a  $\approx 0.03$  eV shift with respect to the monomer, while the two Q<sub>y</sub> bands show no appreciable shift

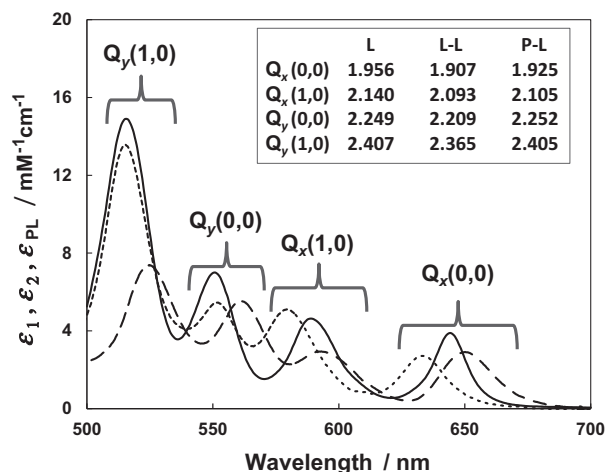


**FIGURE 4.** Limiting normalized absorption spectra (extinction coefficient,  $\varepsilon$ ) for TPPS in the monomeric (short dashed curve), dimeric (long dashed curve) and bound (solid curve) states. Each spectrum consists of four Q bands denoted as Q<sub>x</sub>(0,0), Q<sub>x</sub>(1,0), Q<sub>y</sub>(0,0) and Q<sub>y</sub>(1,0) as we move from high to low wavelengths. The inset shows the corresponding transition energy values in eV associated with the band maxima for the monomer (L), dimer (L-L) and bound (P-L) TPPS.

with respect to the monomer. Since the x axis is located along the direction of the two protonated pyrrole nitrogens of a porphyrin by convention, [46] the observed shifts indicates that the interaction of PVP and TPPS mainly occurs along the x axis. This interaction is expected to involve hydrogen bonding between the two pyrrole hydrogens of TPPS and the PVP oxygens, as indicated by the resonance form in which a negative charge is located on PVP oxygens and a corresponding positive charge on the PVP nitrogens. The  $\pi$  character of the N–C bond may favor  $\pi$ – $\pi$  interactions between polymer and porphyrin.

For completeness, we have also examined the Soret band of TPPS. The corresponding normalized spectra in the UV range are shown in figure 5. Since the intensity of this band is significantly

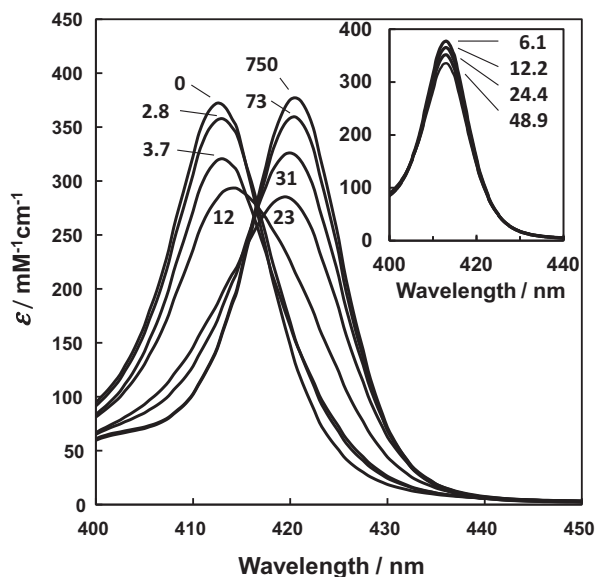


**FIGURE 5.** Normalized absorption spectra (extinction coefficient,  $\varepsilon$ ) showing the Soret band for TPPS (sodium phosphate buffer, 10 mM, pH 7.0, 22.5 °C) at  $C_L = 23$   $\mu\text{M}$  for several PVP concentrations,  $C_P$ . The numbers associated with individual spectra denote the corresponding values of PVP to TPPS concentration ratio,  $C_P/C_L$ . The inset shows normalized absorption spectra for TPPS taken at several  $C_L$  values in the absence of PVP. The numbers associated with individual spectra denote the corresponding  $C_L$  in  $\mu\text{M}$ .

stronger than those of the  $Q$  bands, spectra were collected at relatively low TPPS concentrations. Within this range of dilute concentrations, the effect of TPPS dimerization on the Soret band is small (see inset of figure 5). On the other hand, the effect of PVP on the TPPS Soret band could be clearly investigated resulting into a shift towards high wavelength ( $\approx 0.05$  eV), which is qualitatively consistent with the shift observed for the  $Q_x$  bands.

#### 4. Summary and conclusions

Supramolecular (PVP + TPPS) structures with a maximum molecular weight  $\approx 50\%$  higher than that of the PVP scaffold are obtained in the presence of TPPS concentrations of the order of  $10 \mu\text{M}$  or higher in the surrounding aqueous medium. The comparison between the experimental Van't Hoff plot and that calculated from experimental reaction enthalpies was used to show that TPPS self-association is limited to the formation of dimers and that TPPS binds to PVP in its monomeric state. ITC reaction enthalpies have also allowed us to determine accurate reaction heat capacities. These were related to hydrophobic interactions. Our ITC results show that (PVP + TPPS) binding is stronger than TPPS dimerization due to the difference in reaction entropy. Thermodynamic parameters were used to extract the normalized absorption spectra of monomeric, dimeric and bound states of TPPS. The observed spectral shifts in the two  $Q_x$  bands can be explained by considering that the two hydrogens in the central porphyrin bind to the PVP oxygens.

#### Acknowledgments

This work was supported by the NSF RI Grant (CHE-1126710), TCU Research and Creative Activity Funds and TCU SERC.

#### References

- [1] K.M. Kadish, K.M. Smith, R. Guilard, *The Porphyrin Handbook*, Academic Press, New York, 1999.
- [2] D. Dolphin, *The Porphyrins*, Academic Press, New York, 1978.
- [3] C.J. Medforth, Z. Wang, K.E. Martin, Y. Song, J.L. Jacobsen, J.A. Shelnutt, *Chem. Commun.* 7345 (2009) 7261–7277.
- [4] I. Beletskaya, V.S. Tyurin, A.Y. Tsivadze, R. Guilard, C. Stern, *Chem. Rev.* 109 (2009) 1659–1713.
- [5] M. Gouterman, G.H. Wagnière, *J. Mol. Spectrosc.* 11 (1963) 108–127.
- [6] M. Gouterman, *J. Chem. Phys.* 30 (1959) 1139–1161.
- [7] E.D. Sternberg, D. Dolphin, C. Bruckner, *Tetrahedron* 54 (1998) 4151–4202.
- [8] E.S. Nyman, P.H. Hynninen, *J. Photochem. Photobiol. B Biol.* 73 (2004) 1–28.
- [9] R. Bonnett, *Chem. Soc. Rev.* (1995) 19–33.
- [10] M. Ethirajan, Y. Chen, P. Joshi, R.K. Pandey, *Chem. Soc. Rev.* 40 (2011) 340–362.
- [11] D. Monti, S. Nardis, M. Stefanelli, R. Paolesse, C. Di Natale, A. D'Amico, *J. Sensors* (2009) 1–10.
- [12] L.-L. Li, E.W.-G. Diau, *Chem. Soc. Rev.* 42 (2013) 291–304.
- [13] R.F. Pasternack, P.R. Huber, P. Boyd, G. Engasser, L. Francesconi, E. Gibbs, et al., *J. Am. Chem. Soc.* 94 (1972) 4511–4517.
- [14] L.P.F. Aggarwal, I.E. Borissevitch, *Spectrochim. Acta A Mol. Biomol. Spectrosc.* 63 (2006) 227–233.
- [15] J.M. Ribo, J. Crusats, J. Farrera, M.L. Valero, *J. Am. Chem. Soc. Chem. Commun.* 7 (1994) 681–682.
- [16] R. Rubires, J. Crusats, Z. El-hachemi, T. Jaramillo, M. Lopez, E. Valls, et al., *New J. Chem.* (1999) 189–198.
- [17] J.V. Hollingsworth, A.J. Richard, M.G.H. Vicente, P.S. Russo, *Biomacromolecules* 13 (2012) 60–72.
- [18] O. Ohno, Y. Kaizu, H. Kobayashi, *J. Chem. Phys.* 99 (1993) 4128–4139.
- [19] N. Micalí, F. Mallamace, A. Romeo, R. Purrello, L.S. Monsu, *J. Phys. Chem. B* 104 (2000) 5897–5904.
- [20] M.A. Castriciano, A. Romeo, G. De Luca, V. Villari, L.M. Scolaro, N. Micalí, *J. Am. Chem. Soc.* 133 (2011) 765–767.
- [21] N.C. Maiti, M. Ravikanth, S. Mazumdar, N. Periasamy, *J. Phys. Chem.* 99 (1995) 17192–17197.
- [22] I. Jelesarov, H.R. Bosshard, *J. Mol. Recognit.* 12 (1999) 3–18.
- [23] J.E. Ladbury, G. Klebe, E. Freire, *Nat. Rev. Drug Discovery* 9 (2010) 23–28.
- [24] K. Kano, K. Watanabe, Y. Ishida, *J. Phys. Chem.* 112 (2008) 14402–14408.
- [25] S.R. Vippagunta, A. Dorn, R.G. Ridley, J.L. Vennerstrom, *Biochim. Biophys. Acta* 1475 (2000) 133–140.
- [26] R. Franco, G. Bai, V. Prosiński, F. Abrunhosa, G.C. Ferreira, M. Bastos, *Biochem. J.* 386 (2005) 599–605.
- [27] Y. Egawa, R. Hayashida, J. Anzai, *Langmuir* 23 (2007) 13146–13150.
- [28] P. Dutta, R. Rai, S. Pandey, *J. Phys. Chem. B* 115 (2011) 3578–3587.
- [29] A. Synytsya, A. Synytsya, P. Blafkova, K. Volka, V. Král, *Spectrochim. Acta A Mol. Biomol. Spectrosc.* 66 (2007) 225–235.
- [30] B.K. Manna, D. Sen, S.C. Bera, K.K. Rohatgi-Mukherjee, *Chem. Phys. Lett.* 176 (1991) 191–197.
- [31] S.C.M. Gandini, V.E. Yushmanov, I.E. Borissevitch, M. Tabak, *Langmuir* 15 (1999) 6233–6243.
- [32] N.C. Maiti, S. Mazumdar, N. Periasamy, *Curr. Sci.* 70 (1996) 997–999.
- [33] L. Zhao, R. Ma, J. Li, Y. Li, Y. An, L. Shi, *Biomacromolecules* 9 (2008) 2601–2608.
- [34] K. Kalyanasundaram, M. Neumann-Spallart, *J. Phys. Chem.* 86 (1982) 5163–5169.
- [35] V.G. Kadajji, G.V. Betageri, *Polymers (Basel)* 3 (2011) 1972–2009.
- [36] J. Goldfarb, S. Rodriguez, *Die Makromol. Chem.* 116 (1968) 96–106.
- [37] N.R. Draper, H. Smith, *Applied Regression Analysis*, Wiley, New York, 1966.
- [38] K.E. van Holde, *Physical Biochemistry*, second ed., Prentice-Hall, Englewood Cliffs, NJ, 1985.
- [39] R.B. Martin, *Chem. Rev.* 96 (1996) 3043–3064.
- [40] F. Oosawa, S. Asakura, *Thermodynamics of the Polymerization of Protein*, Academic Press, Waltham, MA, 1975.
- [41] K. Kemnitz, T. Sakaguchi, *Chem. Phys. Lett.* 196 (1992) 497–503.
- [42] K.A. Sharp, B. Madan, *J. Phys. Chem. B* 5647 (1997) 4343–4348.
- [43] Y.B. Yu, P.L. Privalov, R.S. Hodges, *Biophys. J.* 81 (2001) 1632–1642.
- [44] R. Sadeghi, M.T. Zafarani-Moattar, *J. Chem. Thermodyn.* 36 (2004) 665–670.
- [45] V.C.P. da Costa, A.C.F. Ribeiro, A.J.F.N. Sobral, V.M.M. Lobo, O. Annunziata, C.I.A.V. Santos, et al., *J. Chem. Thermodyn.* 47 (2012) 312–319.
- [46] T. Hashimoto, Y.-K. Choe, H. Nakano, K. Hirao, *J. Phys. Chem. A* 103 (1999) 1894–1904.